



11 **Abstract**

12 Ammonia (NH₃) is an important air pollutant which, as precursor of fine particulate matter, raises
13 public health issues. This study analyzes 2.5-years of NH₃ observations derived from ground-based
14 (miniDOAS) and satellite (IASI) remote sensing instruments to quantify, for the first time, temporal
15 variabilities (from interannual to diurnal) of NH₃ concentrations in Paris.

16 The IASI and miniDOAS datasets are found to be in relatively good agreement ($R > 0.70$) when
17 atmospheric NH₃ concentrations are high and driven by regional agricultural activities. Over the
18 investigated period (January 2020 – June 2022), NH₃ average concentrations in Paris measured by the
19 miniDOAS and IASI are 2.23 $\mu\text{g}\cdot\text{m}^{-3}$ and 7.10×10^{15} molecules $\cdot\text{cm}^{-2}$, respectively, which are lower or
20 equivalent to those documented in urban areas. The seasonal and monthly variabilities of NH₃
21 concentrations in Paris are driven by sporadic agricultural emissions influenced by meteorological
22 conditions, with NH₃ concentrations in spring up to 2 times higher than in other seasons.

23 The potential source contribution function (PSCF) reveals that the close (100-200km) east and
24 northeast regions of Paris constitute the most important potential emission source areas of NH₃ in the
25 megacity.

26 Weekly cycles of NH₃ derived from satellite and ground-based observations show different ammonia
27 sources in Paris. In spring, agriculture has a major influence on ammonia concentrations and, in the
28 other seasons, multi-platform observations suggest that ammonia is also controlled by traffic-related
29 emissions.

30 In Paris, the diurnal cycle of NH₃ concentrations is very similar to the one of NO₂, with morning
31 enhancements coincident with intensified road traffic. NH₃ evening enhancements synchronous with
32 rush hours are also monitored in winter and fall. NH₃ concentrations measured during the weekends
33 are consistently lower than NH₃ concentrations measured during weekdays in summer and fall. This is
34 a further evidence of a significant traffic source of NH₃ in Paris.



35 **1. Introduction**

36 Ammonia (NH₃) is an air pollutant which is involved in important environmental and health issues
37 [Rockström et al., 2009]. It is a highly reactive gas, with a lifetime of a few hours to a few days
38 [Evangelidou et al., 2021; Dammers et al., 2019], capable of reacting with nitrogen oxides (NO_x) and
39 sulfur oxides (SO_x) to form fine particulate matter composed of ammonium nitrate and ammonium
40 sulfate [Sutton et al., 2013]. The formation of fine particles plays a major role in the degradation of air
41 quality, as they are the cause of respiratory and cardiovascular diseases [Pope III et al., 2009].

42 Models have difficulty predicting events of particulate pollution associated with NH₃ since ground-
43 based atmospheric observations of this gas are still relatively sparse [Nair and Yu, 2020] and difficult
44 to implement [Twigg et al., 2022; von Bobruzski et al., 2010]. To our knowledge, only six countries in
45 the world (United States, China, the Netherlands, United Kingdom, Belgium, and Canada) have
46 dedicated NH₃ observations in their atmospheric monitoring networks. This poses a problem for long-
47 term monitoring of pollution and the implementation of emission reduction policies.

48 Global population growth causes increased food demand leading to higher ammonia emissions from
49 intensive agricultural production systems [Fowler et al., 2013]. Global NH₃ emissions have increased
50 by more than 80% between 1970 and 2017 [McDuffie et al., 2020]. In Europe, a substantial increase in
51 nitrate and ammonium concentrations in the composition of fine particles has been observed for several
52 years in the early spring when fertilizer applications intensify [Favez et al., 2021]. In addition, the share
53 of emissions related to road traffic is also increasing because of popularization of catalytic converters
54 in car engines [Zhang et al., 2021]. In France, 98% of ammonia comes from agricultural activities, via
55 decomposition and volatilization of nitrogen fertilizers (34%) and animal waste (64%), the rest are from
56 industry, road traffic and residential heating [CITEPA, 2022]. In the Ile-de-France region (Paris greater
57 area), the share of agriculture is lower (75%) due to a higher contribution of traffic and residential
58 sectors (13% and 12%, respectively [AirParif, 2022]). NH₃ emissions from road traffic are very poorly
59 quantified and may be a larger than expected source in urban areas [Pu et al., 2023; Chatain et al.,
60 2022; Cao et al., 2021; Roe et al., 2004; Sutton et al., 2000].

61 Monitoring NH₃ is therefore essential, especially in urban areas such as in Paris, where particulate
62 pollution episodes are monitored almost every spring [Viatte et al., 2021; Viatte et al., 2020; Petetin
63 et al., 2016].

64 Global scale measurement of atmospheric ammonia is possible via soundings from several satellite-
65 borne instruments such as AIRS [Warner et al., 2016], CrIS [Shephard and Cady-Pereira, 2015], and IASI
66 [Clarisse et al., 2009]. Satellite measurements of atmospheric ammonia allow a description of its spatial
67 distribution with global coverage. The detection of the multi-year evolution of concentrations is
68 possible, as well as the detection of emission sources at the kilometer scale [Van Damme et al., 2018],
69 and even the quantification of their variabilities [Van Damme et al., 2021; Dammers et al., 2019].
70 Remote sensing data are also used as a mean to estimate ammonia emission inventories [Marais et
71 al., 2021; Cao et al., 2020; Fortems-Cheiney et al., 2020].

72 Quantifying and analyzing temporal NH₃ variabilities at different scales (diurnal, weekly, seasonal, and
73 interannual) helps to improve emission inventories and air quality forecasts [Cao et al., 2021]. Diurnal
74 NH₃ variability, which is rarely measured, is particularly crucial because atmospheric models have
75 difficulty representing it [Lonsdale et al., 2017]. NH₃ concentrations increase during the day due to the
76 temperature dependence of emissions, but there may be many other factors at play influencing the



77 diurnal variability of NH_3 concentrations in the atmosphere, such as transport, boundary layer height,
78 deposition, fertilizer application time, road traffic emissions, and the interaction of all these factors
79 [Sudesh and Kulshrestha, 2021; Osada, 2020; Wang et al., 2015]. The diurnal variability of NH_3 , which
80 is still largely missing from the ground and satellite observations, provides valuable information
81 regarding sources, surface exchange, deposition, gas-particle conversion, and transport of NH_3
82 [Clarisse et al., 2021].

83 In this work, we present 2.5-years of atmospheric NH_3 concentrations measured in Paris using the
84 synergy of ground-based and IASI satellite observations to quantify NH_3 variabilities at different time
85 scales.

86 **2. Methodology**

87 **2.1. mini-DOAS**

88 The miniDOAS (Differential Optical Absorption Spectroscopy) is a state-of-art instrument suitable for NH_3
89 monitoring [Berkhout et al., 2017] since it performs accurate high temporal resolution measurements
90 (every hour, day and night) [Volten et al., 2012]. It has been designed and developed by the National
91 Institute for Public Health and the Environment (RIVM, Netherlands) to be part of the Dutch National
92 Air Quality Monitoring Network [Berkhout et al., 2017]. The miniDOAS is an active remote sensing
93 instrument based on open-path differential absorption spectrometry. It uses a xenon lamp which emits
94 a UV light, ammonia having a strong absorption band in the UV between 200 and 230 nm. The UV light
95 beam travels along an optical path of 20 m, at the end of which there is a reflector which reflects the
96 UV light and sends it back to the spectrometer/receiver. The Beer-Lambert law is used to quantify the
97 extinction at the absorption wavelengths of ammonia to retrieve atmospheric ammonia
98 concentrations [Volten et al., 2012]. The miniDOAS can measure a wide range of ammonia
99 concentrations (from 0.5 to 200 $\mu\text{g.m}^{-3}$) day and night with no sampling artifacts, since it is not using
100 any filter or inlet unlike other instruments [Caville et al., 2023; von Bobruzki et al., 2010]. Estimated
101 errors are $4.10^{-3} \mu\text{g.m}^{-3}$ on hourly measurements [Volten et al., 2012]. Using ammonia measurements
102 performed from the miniDOAS at the QUALAIR super-site (40 meters above ground level,
103 <https://qualair.fr/index.php/en/english/>) in the Paris city-center, the NH_3 contribution in particulate
104 pollution events that occurred during the 2020 COVID lockdown has been demonstrated [Viatte et al.,
105 2021].

106 **2.2. IASI**

107 The Infrared Atmospheric Sounding Interferometer (IASI, [Clerbaux et al., 2009]) was launched first in
108 2006 as part of the Metop satellite series to monitor atmospheric composition twice a day (at 9:30 and
109 21:30) globally. IASI measures atmospheric spectra in the thermal infrared region with an elliptical
110 pixel footprint of 12×12 km at nadir and 20×39 km at the far end of the swath. In this study, we use
111 NH_3 columns derived from IASI morning (9:30) overpasses onboard Metop B and C from January 2020
112 to June 2022. When comparing IASI and miniDOAS NH_3 concentrations in Paris, we have selected
113 coincident observations made within the same hour. In this work, we use version 3 of the ANNI- NH_3
114 reanalyzed dataset [Van Damme et al., 2021; Guo et al., 2021; Viatte et al., 2022].

115 **2.3. Meteorological data from ERA-5**

116 Meteorological parameters originate from the ERA-5 database of the European Centre for Medium-
117 Range Weather Forecasts (ECMWF, [Hersbach et al., 2020]). It is constituted from observations



118 recalibrated on global data assimilation models at a 30km spatial resolution. In this work, we used the
119 hourly data of the temperature at 2 m, the precipitation, the u and v components of the wind at 100
120 m and the height of the boundary layer, taken from the grid cells in which Paris is located.

121 **2.4. Back-trajectories and Potential Source Contribution Factor (PSCF) analysis**

122 To study the transport affecting concentration of ammonia in Paris, we use the Hybrid Single-Particle
123 Lagrangian Integrated Trajectory model (HYSPLIT, [Stein et al., 2015]) to calculate backward
124 trajectories of air masses ending at altitudes of 100 m (above sea level which corresponds to the
125 altitude of the miniDOAS location) between January 2020 and June 2022.

126 Meteorological data used in the runs are from the National Centers for Environmental Prediction
127 (NCEP) / National Center for Atmospheric Research (NCAR) reanalysis at 2.5-degree global latitude-
128 longitude projection. We ensure by visual inspections that the back trajectories using a 2.5° resolution
129 meteorological dataset are similar to using a finer meteorological dataset at 0.25° resolution (GFS).

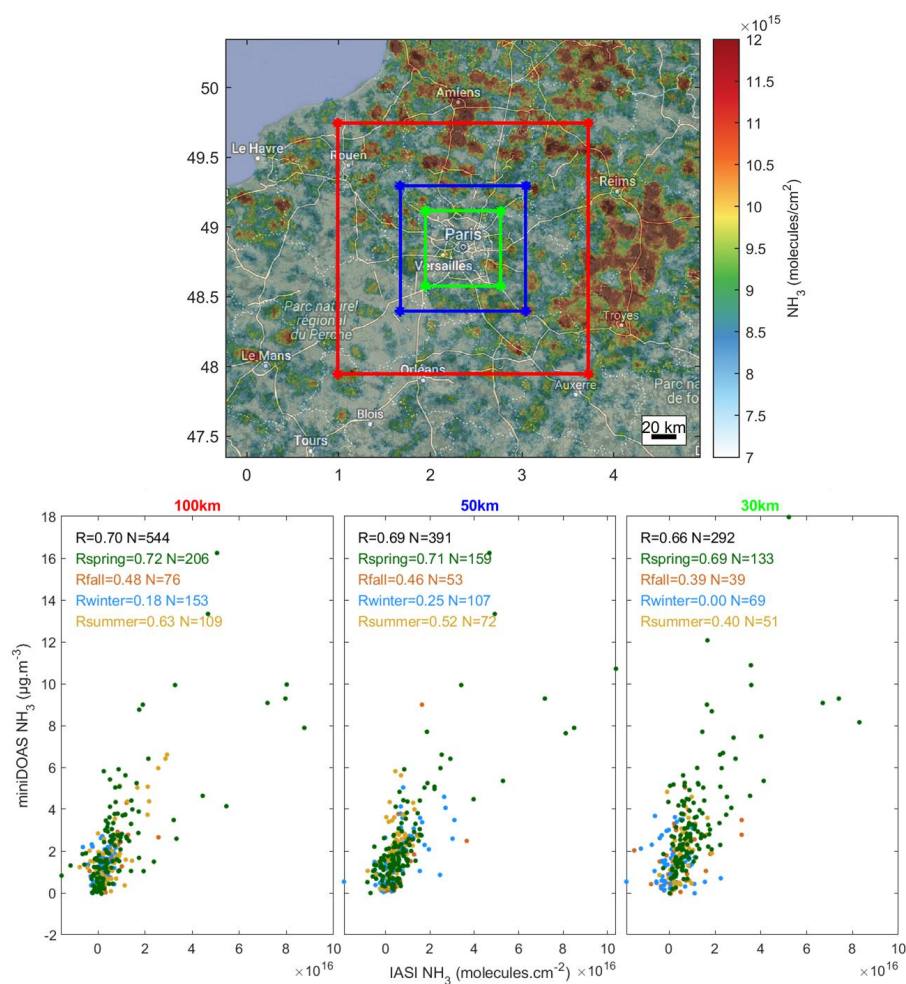
130 Due to the short and highly variable lifetime of NH₃, ranging between 2-4 hours [Dammers et al., 2019]
131 and 12-hours [Evangelidou et al., 2021], we simulated an average 6-h backward trajectories with an
132 interval of one hour. Combining the hourly NH₃ observations from the miniDOAS, the potential
133 emission sources of NH₃ were analyzed. The Potential Source Contribution Factor (PSCF) method
134 [Malm et al., 1986] is used to identify source regions affecting air quality in term of NH₃ concentration
135 in Paris between January 2020 and June 2022. This method is now commonly used in atmospheric
136 science [Wang et al., 2023; Qadri et al., 2022; Martino et al., 2022; Biuki et al., 2022; Ren et al., 2021;
137 Zachary et al., 2018; Jeong et al., 2011] and combines the concentration dataset with air parcel back-
138 trajectory to identify preferred pathways producing high observed NH₃ concentrations in Paris. The
139 larger PSCF (range: 0–1), the greater contribution of the pollution region to the atmospheric pollutants
140 at the receptor site.



141 **3. Results**

142 **3.1. Comparison of NH₃ concentrations between IASI and mini-DOAS**

143 The 2.5-years mean NH₃ total column distribution around Paris derived from IASI from January 1st 2020
 144 to May 31st 2022 is shown in Figure 1 (top panel). To obtain averages at a high resolution needed for
 145 city-scale studies, we used the oversampling method that takes into account the real elliptical sizes of
 146 each IASI pixel [Van Damme et al., 2018]. Hot spots of ammonia are found around Paris in agricultural
 147 areas, especially in the Champagne-Ardennes region between Troyes and Reims cities [Viatte et al.,
 148 2020].



149

150 *Figure 1: Top panel: 2.5-years average of IASI NH₃ column distributions (from January 1st 2020 to May*
 151 *31st 2022). Bottom panel: miniDOAS ground-based NH₃ concentrations (µg.m⁻³) versus IASI-retrieved*
 152 *NH₃ column concentrations (molecules.cm⁻²) per season for different spatial criteria from Paris city*
 153 *center where the miniDOAS is located (100km in red box, 50km in blue box, and 30km green box).*



154 NH₃ has a short atmospheric lifetime which is why we only compare miniDOAS data recorded within
155 the same hour as the IASI morning overpass time. The IASI-retrieved column (in molecules.cm⁻²) and
156 the miniDOAS ground-based concentrations (µg.m⁻³) are qualitatively compared to assess the spatial
157 criteria (100km in red box, 50km in blue box, and 30km green box) and the season for which both
158 datasets are in best agreement. In this study we are not converting IASI columns to surface
159 observations since it introduces additional errors and does not change the correlation as explained in
160 [Van Damme et al., 2015].

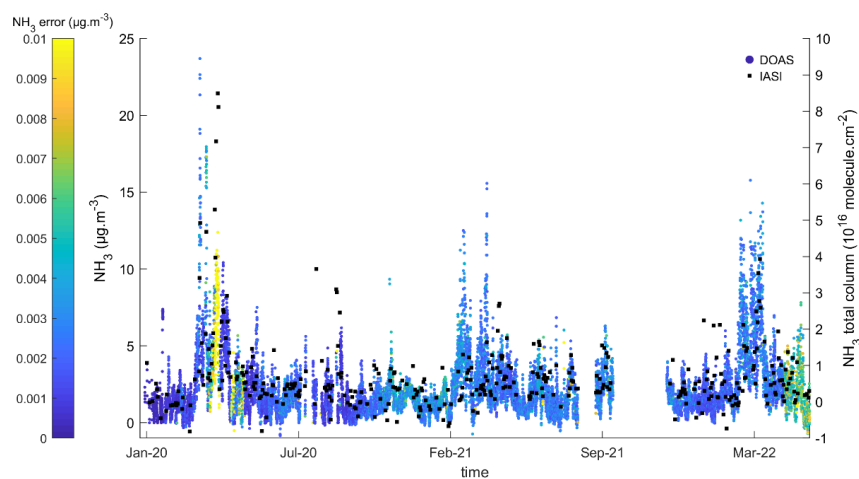
161 Overall, the miniDOAS and IASI NH₃ concentrations are in moderate agreement with Pearson
162 correlation [Akoglu et al., 2018] of 0.70, 0.69, and 0.66 when considering IASI pixels within a 100km,
163 50km, and 30km box around Paris, respectively. The number of pairs is, however, reduced by a factor
164 of two when considering IASI pixels in a 100km versus a 30km box around Paris. All correlations are
165 significant (p-value < 0.05) except in winter for the 100km and 30km boxes, and in fall for the 30km
166 box. The best agreement between the miniDOAS and IASI is in spring, with Pearson correlations ranging
167 from 0.72 to 0.69 (green points in scatter plots of Figure 1). This period corresponds to high
168 atmospheric NH₃ concentrations when spreading practices occur in the surrounding agricultural
169 regions of Paris [Viatte et al., 2022]. In fall and summer, the Pearson correlation coefficients range
170 from 0.63 to 0.40 between IASI and the miniDOAS for all boxes sizes. In winter, the agreements are
171 poor between the miniDOAS and IASI because NH₃ concentrations are weak and IASI is less sensitive
172 to lower atmospheric layers when thermal contrast is low [Van Damme et al., 2014]. In addition, we
173 demonstrate that correlations between satellite and ground-based NH₃ observations are independent
174 of atmospheric temperature and planetary boundary layer height (PBLH, Figure S1).

175 A trade-off between good correlations and keeping a sufficient number of collocations is found when
176 comparing NH₃ concentrations from ground-based measurements located in the Paris city-center with
177 the IASI dataset in a 50 km box. We chose for the rest of the analysis IASI dataset within the 50 km box
178 to analyze spatiotemporal variabilities of NH₃ in Paris.

179 **3.2. Impact of agriculture on NH₃ concentrations in Paris**

180 **3.2.1 2.5-years of NH₃ measurements in Paris**

181 Here, we investigate temporal variabilities of NH₃ using 2.5-years of hourly measurements from
182 January 1st 2020 to May 31st 2022 (Figure 2). The miniDOAS was working almost full time during this
183 period with 16 888 hourly measurements, out of the 21 145 possible. The missing data is due either to
184 some technical issues during warm conditions (malfunctioning aircondition in August 2021) or due to
185 its removal from the QUALAIR facility for field measurement campaigns (from September 15th 2021 to
186 November 24th 2021). Over the 16 888 hourly NH₃ measurements, average errors are 2.8 10⁻³ µg.m⁻³
187 with maximum values occurring when signal is low due to a transient poor alignment (such as in April
188 2020, yellow dots in Figure 2).



189

190 *Figure 2: Timeseries of hourly NH₃ concentrations (in µg.m⁻³) color coded by the errors on*
 191 *measurements derived from the miniDOAS located in Paris, and IASI NH₃ total columns (in black,*
 192 *molecule.cm⁻²) observed in a 50km box centered in Paris from January 1st 2020 to May 31st 2022.*

193 The measurements made by the miniDOAS over the period January 2020 - June 2022 (N=16 888) show
 194 an average ammonia concentration of 2.23 µg.m⁻³ in Paris over this period, with a standard deviation
 195 of 2.02 µg.m⁻³, indicating a high NH₃ variability. In comparison, the average concentration measured
 196 by the miniDOAS in an agricultural site at Grignon [Loubet et al., 2022] in September–October 2021
 197 (France) is 6.52 ± 8.44 µg.m⁻³ [Claville et al., 2023], almost three times higher than in Paris. The
 198 relatively low concentrations observed in Paris are explained by the distance to the major emission
 199 sources which are related to agricultural activities. Ammonia concentrations measured in Paris are on
 200 average lower or equivalent to those documented in urban areas such as Beijing (China, 21 ± 14 ppb
 201 corresponding to 14.7 ± 10 µg.m⁻³ from January 2018 to January 2019, [Lan et al., 2021]), Shanghai
 202 (China, 6.2 ± 4.6 ppb which corresponds to 4.3 ± 3.2 µg.m⁻³ from July 2013 to September 2014, [Wang
 203 et al., 2015]), Rome (Italy, 1.2–21.6 µg.m⁻³ between May 2001 and March 2002, [Perrino et al., 2002]),
 204 Milan (Italy, 4.4–13.4 µg.m⁻³ between 2007 and 2019, [Lonati et al., 2020]), Louisville (Unites-States,
 205 2.2–5.2 µg.m⁻³ from June to August 2011, [Li et al., 2017]) and Toronto (Canada, 2.5 ppb which
 206 corresponds to 1.75 µg.m⁻³ from 2003 to 2011, [Hu et al. 2014]).

207 The miniDOAS and IASI coincident measurements show relatively low interannual variability (Table 1).
 208 NH₃ annual concentrations measured by the miniDOAS are 2.06 ± 2.09 µg.m⁻³ and 2.04 ± 1.56 µg.m⁻³
 209 for 2020 and 2021, respectively. The higher mean and standard deviation in 2022 (2.91 ± 2.40 µg.m⁻³
 210 for the miniDOAS) compared to the other years can be due the fact that measurements are performed
 211 from January to June only. IASI NH₃ total columns around Paris exhibit a higher NH₃ annual
 212 concentration and standard deviation in 2020 compared to the other years because of high pollution
 213 events occurring in spring during the 2020-COVID lockdown [Viatte et al., 2021].



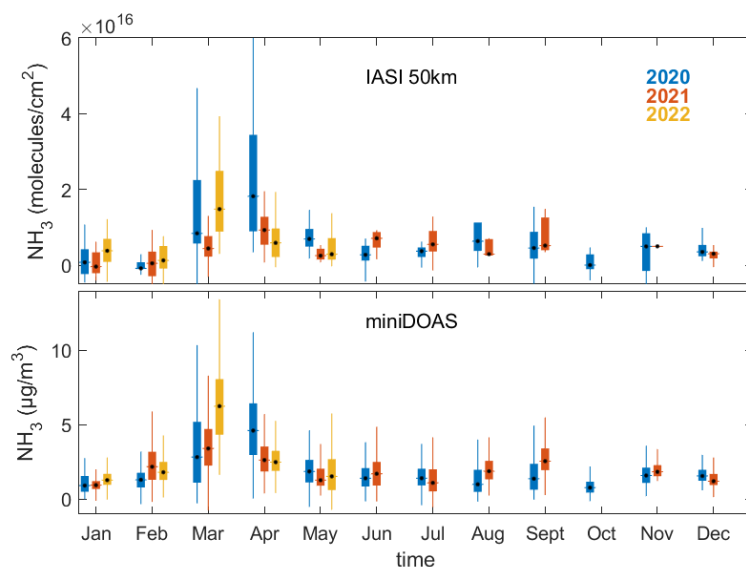
214 *Table 1: Average NH₃ concentration, standard deviation, and number of observations for 2020, 2021*
 215 *and part of 2022 derived from coincident measurements of the miniDOAS and IASI (50 km box around*
 216 *Paris).*

years	2020		2021		2022	
	miniDOAS	IASI (50km)	miniDOAS	IASI (50km)	miniDOAS	IASI (50km)
NH ₃ concentration (µg.m ⁻³ or molecules.cm ⁻²)	2.06	8.60 10 ¹⁵	2.04	5.48 10 ¹⁵	2.91	6.76 10 ¹⁵
Standard deviation (µg.m ⁻³ or molecules.cm ⁻²)	2.09	1.58 10 ¹⁶	1.56	5.69 10 ¹⁵	2.40	9.35 10 ¹⁵
Number of observations	7164	166	6182	134	3542	91

217

218 3.2.2 Seasonal and monthly NH₃ variabilities in Paris

219 Unlike the weak interannual variability of NH₃ concentrations in Paris, both ground-based (miniDOAS)
 220 and satellite (IASI) measurements reveal high seasonal variabilities of NH₃ concentrations (Figure 3). In
 221 spring, NH₃ concentration measured in Paris by the miniDOAS and IASI are on average
 222 $3.34 \pm 2.67 \mu\text{g.m}^{-3}$ and $1.21 \times 10^{16} \pm 1.57 \times 10^{16}$ molecules.cm⁻², respectively. These springtime NH₃
 223 concentrations are enhanced by a factor of two compared to the other seasons, which is consistent
 224 with the fertilizer application periods over the nearby agricultural fields. Both datasets show that NH₃
 225 concentrations in March and April are 2 to 3 times higher than the other months. Precipitation for
 226 these months is also lower than in February on average (see supplementary Figure S2).



227

228 *Figure 3: Monthly NH₃ concentrations color coded by the year of measurements (2020 in blue, 2021 in*
 229 *orange, and 2022 in yellow) derived from IASI (top panel, in molecules.cm⁻²) in a 50km box around Paris*
 230 *and the ground-based miniDOAS instrument (bottom panel, in µg.m⁻³) located in Paris city-center. One*
 231 *note that IASI observations are only considered when a miniDOAS observation is available within the*
 232 *same hour than IASI overpass.*



233 When considering each year of measurement separately, we notice that the timing of the maximum
234 NH_3 concentrations is variable. In 2020, the maximum is reached in April with averaged NH_3
235 concentrations of $4.76 \pm 2.48 \mu\text{g.m}^{-3}$ (miniDOAS) and $2.90 \times 10^{16} \pm 2.85 \times 10^{16}$ molecules. cm^{-2} (IASI),
236 whereas in 2022 the maximum appears in March with a monthly NH_3 concentration of 6.42 ± 2.46
237 $\mu\text{g.m}^{-3}$ and $1.72 \times 10^{16} \pm 1.04 \times 10^{16}$ molecules. cm^{-2} derived from the miniDOAS and IASI, respectively.

238 Meteorological conditions influence the timing of the agricultural practices (farmers do not spread
239 their fertilizer when it rains), NH_3 volatilization from the soil to the atmosphere (higher temperature
240 favors NH_3 volatilization [Sutton et al., 2013]), and the transport of NH_3 over Paris.

241 In April 2020, NH_3 concentrations observed by IASI and the miniDOAS are high compared to April 2022.
242 In April 2020, precipitation is low (0.3 mm compared to 0.75mm in April 2022) and the monthly
243 averaged atmospheric temperature is on 3 to 5°C higher than in 2021 and 2022 (Figure S2). This could
244 explain why NH_3 concentrations are higher in April 2020 than in 2022. Similarly, the lower ammonia
245 concentration recorded in March 2021 compared to March 2022 is likely explained by higher
246 precipitation (0.09 mm) and a lower temperature (of 2°C on monthly average) than in March 2022.

247 In 2021, a second NH_3 enhancement is measured in September by the miniDOAS ($2.73 \pm 1.14 \mu\text{g.m}^{-3}$)
248 and IASI ($7.93 \times 10^{15} \pm 4.64 \times 10^{15}$ molecules. cm^{-2}). The pronounced seasonal variability can be explained
249 in the first order by the practices of the farmers. In most European countries, strict regulations are
250 applied in term of the timing of fertilizer application [Ge et al., 2020]. In France, it is forbidden to spread
251 nitrogen fertilizers in winter months (between November 30th and February 15th, [Ludemann et al.,
252 2022]) depending on fertilizer and land/crop types.

253 Overall, the seasonal and monthly variabilities of NH_3 concentrations in Paris are dominated by
254 agricultural activities and meteorological conditions.

255 **3.2.3 Potential Source Contribution Function (PSCF) analysis for NH_3 concentrations**

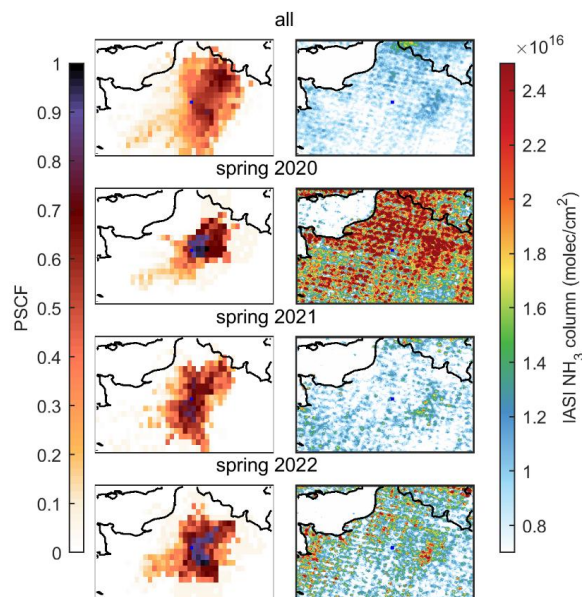
256 To determine the origin of the NH_3 measured in Paris, the Potential Source Contribution Function
257 (PSCF) is used. The PSCF analysis, as well as the IASI NH_3 maps, are shown for the investigated period
258 (January 2020 – June 2022, Figure 4 upper panels), and for springs 2020, 2021, and 2022 (Figure 4,
259 three lower panels).

260 Over the whole timeseries, the northeast (100 km from Paris in the Aisne department of France) and
261 east (70km from Paris in the “Seine et Marne” department) locations are found to affect the NH_3
262 concentrations observed in the city between January 2020 and June 2022. These areas are indeed
263 source regions of NH_3 according to coincident IASI observations (Figure 4, upper panels). According to
264 wind fields parameters derived from ERA-5 over Paris (not shown here), the winds from the south are
265 more intense (up to 18 m.s^{-1}) and are related to lower ammonia concentrations (between 0 and 4 $\mu\text{g.m}^{-3}$).
266 The northern winds are on average weaker (maximum around 12 m.s^{-1}) and are associated with
267 higher ammonia concentrations. In particular, for the northeast section the measured NH_3
268 concentration is found to exceed 8 $\mu\text{g.m}^{-3}$.

269 According to the PSCF analysis, the main sources of NH_3 from agricultural activities are found in the
270 close areas of Paris (within 100 and 200 km from Paris city-center) mainly from the east and northeast
271 directions. In France, the averaged utilized agricultural area per department in 2020 is 64.5 ha (Agreste
272 – Recensements agricoles, <https://stats.agriculture.gouv.fr/cartostat/#c=home>). The highlighted



273 departments by the PSCF analysis are ranked to have the most cultivated areas in France with 141.5
274 ha for Seine et Marne, 124.4 ha for Oise, and 110.4 ha for Aisne departments for instance.
275



276
277 *Figure 4: Potential Source Contribution Function (PSCF, left) and IASI NH₃ total columns (right, in*
278 *molecules.cm⁻²) The top row is the January 2020 to June 2022 average, and the 3 lower panels are for*
279 *springs 2020, 2021, and 2022. The blue dot indicates the location of Paris.*

280 In spring, when NH₃ concentrations are significantly higher in Paris (Figure 3) and in the surroundings
281 (Figure 4 three lower right panels), the PSCF analysis show that the northeast and southeast regions
282 are the major sources of the observed NH₃ concentrations in Paris. In spring 2020, NH₃ columns are
283 higher than in spring 2021 and 2022, according to IASI observations. The main sources of NH₃ in spring
284 2020 are pronounced in the nearby east-northeast areas (at 50 km from Paris in the surrounding
285 departments of Seine et Marne, Oise, and Val d'Oise). In spring 2021, IASI observations reveal lower
286 NH₃ columns than in 2020 and 2022 and the sources of NH₃ concentrations in Paris are in the
287 surrounding regions of Paris (100 km in all directions). In spring 2022, the northeast pathway is
288 highlighted similarly to spring 2020 but with a contribution of the southeast region as well.



289 **3.3 Effect of road traffic on NH₃ variability in Paris**

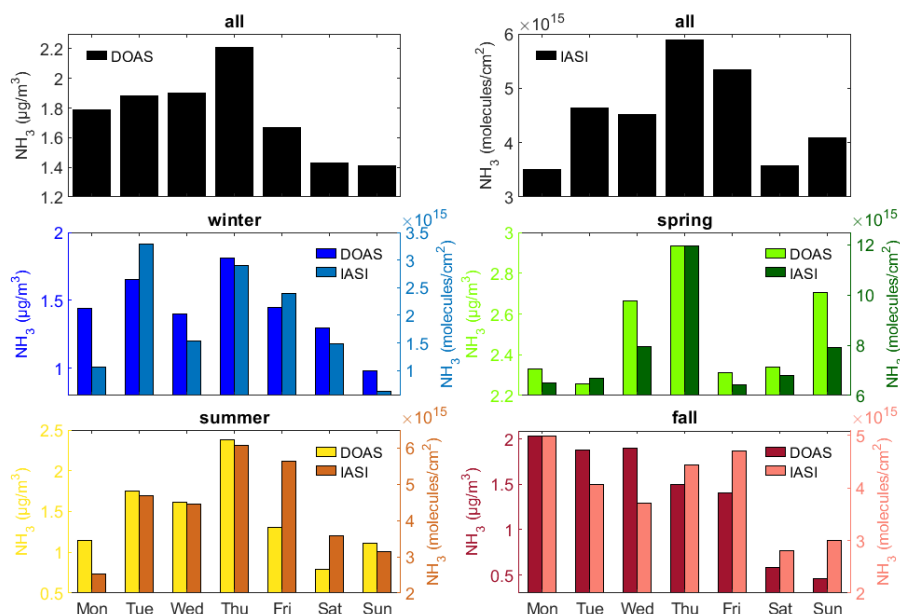
290 **3.3.1 Weekly cycle of NH₃ concentrations**

291 The weekly cycles of ammonia concentrations measured in Paris by the miniDOAS and IASI over the
292 studied timeseries are presented in Figure 5 (black bars, top panels). Both datasets show an increase
293 of ammonia concentrations during the week, reaching a maximum on Thursday (2.21 µg.m³ for the
294 miniDOAS and 5.90x10¹⁵ molecules.cm⁻² for IASI).

295 The weekly cycle of IASI measurements in Paris is almost analogous to the one observed over European
296 agricultural areas with low concentrations observed on Mondays and an accumulation of ammonia
297 during the week [Van Damme et al., 2022]. In addition, the IASI NH₃ weekly cycle averaged over 2.5-
298 years of measurements in Paris is very similar to the NH₃ weekly cycle measured in spring (Figure 5)
299 when agricultural activities intensify. Monitoring similar NH₃ weekly variability in the urban area of
300 Paris demonstrates that agricultural activities in the surrounding areas control the variability of
301 ammonia in Paris on average over the whole season.

302 The NH₃ weekly cycle observed over 2.5-years of measurements from the ground-based miniDOAS and
303 the IASI satellite observations show, however, relatively low NH₃ concentrations on Saturday and
304 Sunday. The cycle is less pronounced for IASI measurements. Ammonia concentrations observed over
305 the weekend by the miniDOAS and IASI are lower by 25% and 20% compared to NH₃ concentrations
306 averaged over the weekdays in Paris.

307 When considering intraweek variabilities by seasons (Figure 5, four lower panels), one can observe
308 that both IASI and the miniDOAS dataset reveal similar NH₃ weekly cycles. The NH₃ miniDOAS
309 measurements and coincident IASI total columns measured in a 50km box around Paris exhibit lower
310 concentrations over the weekends compared to weekdays for all seasons, except in spring for which
311 higher NH₃ concentrations are found on Wednesday and Sunday. In spring, the miniDOAS and IASI
312 measure a difference of NH₃ concentrations averaged over the weekends compared to weekdays of
313 +1% and -7%, respectively. In fall, summer, and winter, the miniDOAS (IASI) instrument measure a
314 decrease of NH₃ concentrations between weekends and weekdays of 70% (34%), 42% (28%), and 27%
315 (53%) respectively.



316

317 *Figure 5: Day of the week NH₃ concentrations derived from the miniDOAS ($\mu\text{g}\cdot\text{m}^{-3}$) and IASI*
 318 *(molecules.cm⁻²) in Paris for the investigated period (January 2020 to May 2022, top panels), and for*
 319 *different seasons (winter in blue, spring in green, summer in brown and yellow, and fall in red and pink*
 320 *bars).*

321 Comparing these weekly variabilities with those of the weekly flow of cars in Paris (Figure S3), the same
 322 pattern is clearly highlighted with a stable number of cars per hour from Monday to Friday (around
 323 640) and a decrease of 14% over the weekends.

324 We can make the hypothesis that during all seasons except spring, the influence of the agricultural
 325 practices on the variability of ammonia in Paris is less pronounced, revealing NH₃ contribution from
 326 the traffic source. Since the road traffic intensity is constant throughout the year in Paris, the
 327 proportion of ammonia emitted from road traffic is proportionally higher outside the fertilization
 328 period.

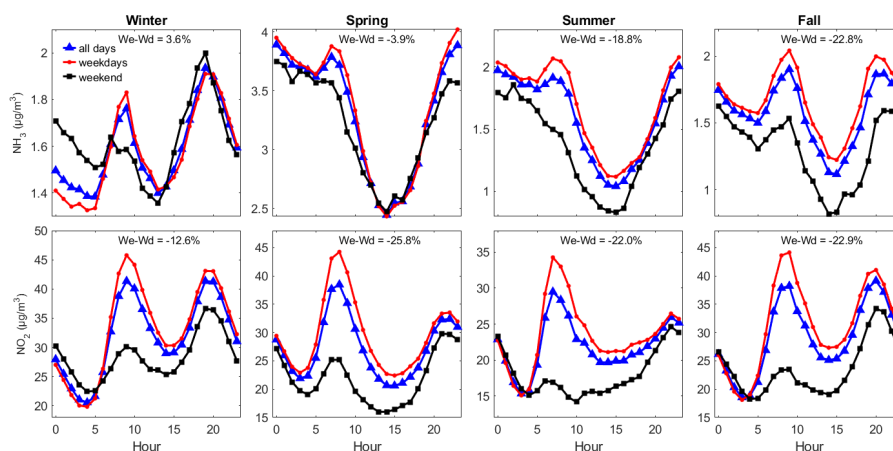
329 3.3.2 Diurnal cycle of NH₃ concentration in Paris

330 With the high temporal resolution of the mini-DOAS acquisitions, the diurnal variability of NH₃
 331 concentration is assessed in Paris using, for the first time, a quasi-continuous (temporal coverage of
 332 80%) and a relatively long timeseries of 2.5-years of NH₃ observations.

333 Hourly NH₃ concentrations measured by the miniDOAS from January 2020 to May 2022 are shown in
 334 Figure S4. It shows a marked diurnal variability of NH₃, with a decrease of about 30% in the middle of
 335 the day (around 14:00 LT) compared to the night, then an increase in the afternoon to reach again a
 336 maximum during the night.



337 Note that this diurnal variability of NH_3 measured by the miniDOAS is different than the one reported
 338 during springtime pollution episodes from a ground-based Fourier Transform InfraRed spectrometer
 339 located in the suburbs of Paris [Kutzner et al., 2021]. While measured integrated NH_3 total columns
 340 show an intraday increase until late afternoon, the miniDOAS measures NH_3 concentrations varying in
 341 opposition to the boundary layer height (Figure S4). This reflects the dynamical effect of the boundary
 342 layer height, which is controlled by atmospheric temperature, on the dilution of pollutants
 343 concentrations measured close to the surface. Such effect is also seen with surface measurements of
 344 NO_2 concentrations in Paris (Figure S4).



345

346 *Figure 6: Diurnal variability of NH_3 (upper panels) and NO_2 (lower panels) concentrations measured by*
 347 *the miniDOAS and Airparif in ($\mu\text{g}\cdot\text{m}^{-3}$) averaged by seasons using 2.5-years of measurements in Paris.*
 348 *Hours are indicated in local time. The diurnal variability of NH_3 and NO_2 are shown in blue lines when*
 349 *considering all days, in red lines for weekdays, and in black lines for weekends.*

350 The diurnal variability of NH_3 concentrations presents an increase in the morning visible for all seasons
 351 (Figure 6). Between 5:00 and 8:00, road-traffic in Paris increases by a factor 4 (Figure S3) and NH_3
 352 concentrations rise by more than 20% in winter and fall, and about 3% in summer and spring.

353 To verify the hypothesis that road traffic is responsible for these morning enhancements, NO_2 diurnal
 354 variability is also shown in Figure 6 (lower panels). In Paris, NO_2 is considered as a proxy for road traffic
 355 emissions [Pazmino et al., 2022]. For all seasons, morning enhancements of NO_2 concentrations related
 356 to intensified road traffic emissions are coincident with morning enhancements of NH_3 concentrations.
 357 Similarly, enhancements of NO_2 and NH_3 concentrations are observed during the evenings (20:00 to
 358 22:00 LT) in winter and fall only. In spring, agriculture which is the overall dominant source of ammonia
 359 in Paris, prevents from monitoring NH_3 emitted from road traffic. Conversely, in fall and winter, the
 360 relative share of agriculture is weaker, and the peaks of NH_3 concentrations during rush hours (morning
 361 and evening) are clearly observed by the miniDOAS.

362 Diurnal variability of NH_3 and NO_2 concentrations averaged during weekdays (red lines) and weekends
 363 (black lines) are shown in Figure 6. NO_2 concentrations are systematically lower during weekends by
 364 12.6%, 25.8%, 22.0%, and 22.9% in winter, spring, summer, and fall respectively, compared to



365 weekdays. Similarly, diurnal cycle of NH_3 concentrations averaged during weekends are constantly
366 lower than NH_3 concentrations averaged during weekdays in summer and fall by 22.0% and 22.9%.

367 This highlights the importance of traffic emissions of NH_3 in such urban area of Paris, detected by
368 ground-based measurements when agricultural practices are reduced in the surrounding region.

369 These results are consistent with previous studies showing the importance of NH_3 emissions from
370 traffic in urban areas, such as in Rome (Italy, [Perrino et al., 2002]), in Beijing (China, [Ianniello et al.,
371 2010]), in Shanghai (China, [Wang et al., 2015]), and in Manchester (United Kingdom, [Whitehead et
372 al., 2004]) for instance. These emissions have gradually become another major contribution of
373 ammonia pollution in urban areas in the United States and China [Sun et al., 2017]. Ammonia emissions
374 from road vehicles are shown to be underestimated in the United Kingdom [Farren et al., 2020] and in
375 densely-populated areas in China [Wen et al., 2022]. In France, NH_3 levels measured at a traffic site are
376 significantly higher than those observed in a background site [Chatain et al., 2022]. Our results in Paris
377 confirm that traffic has a significant contribution to atmospheric nitrogen budgets and stress the need
378 for further NH_3 monitoring in urban sites.

379 **4. Conclusion**

380 Atmospheric variabilities of NH_3 concentrations in Paris are assessed using joined observations of
381 ground-based (miniDOAS) and satellite (IASI) remote sensing observations from January 2020 to June
382 2022. We present the first relatively long (2.5-years) and continuous record of hourly NH_3
383 concentrations in Paris to determine temporal variabilities of ammonia at different scales (from
384 interannual to diurnal variability) to unravel emission sources (traffic and agriculture).

385

386 Qualitative comparison of NH_3 derived from the ground-based miniDOAS located in Paris city-center
387 and IASI satellite observations reveals an overall moderate agreement with Pearson's correlation
388 coefficients of 0.66, 0.69 and 0.70 when considering IASI observations in a 100km, 50km, and 30km
389 box around Paris. The best agreement between both datasets is found during springtime when NH_3
390 concentrations are 2 to 3 times higher than during the other seasons due to spreading practices
391 occurring in the surrounding agricultural regions of Paris. Overall, agricultural activities driven by
392 favorable meteorological conditions (high temperature and low precipitation) control the seasonal and
393 monthly variabilities of NH_3 in Paris. The PSCF analyses indicate that the close east and northeast
394 agricultural regions (within 100 and 200 km from Paris city-center) affect the most the NH_3 budget in
395 Paris.

396

397 Road-traffic emissions are noticeable in the weekly NH_3 cycles measured by satellite and ground-based
398 instruments, when agricultural related emissions are weak. Ammonia concentrations observed over
399 the weekend by the miniDOAS and IASI are lower by 25% and 20% compared to NH_3 concentrations
400 averaged over the weekdays. In addition, diurnal cycles of NH_3 concentrations in Paris are similar to
401 NO_2 and reveal coincident enhancements during rush hours. Further long-term NH_3 monitoring in
402 urban areas is needed to better estimate NH_3 emissions from the on-road sector and their impact on
403 secondary particle formation.

404

405 We have shown that the planetary boundary layer height greatly influences diurnal variabilities derived
406 from surface measurements. Future work will be carried to compare these NH_3 datasets in Paris to
407 atmospheric model outputs to evaluate the timing and the absolute value of emission inventories, as



408 well as the partition between NH₃ emission sectors (traffic vs. agriculture). The launch of the
409 geostationary MTG satellite carrying the hyperspectral sounder IRS, scheduled for 2024, will offer
410 unprecedented atmospheric observations with a spatial resolution of 4 km × 4 km (at the Equator) and a
411 high temporal resolution (every 30 minutes over Europe). These new observations will improve our
412 understanding of the diurnal variability of ammonia, and it will be a great addition to the miniDOAS
413 and IASI observations.

414

415 **Data availability**

416 The IASI NH₃ dataset used in this study are available via the Zenodo repository
417 <https://doi.org/10.5281/zenodo.7962362> (Viatte, 2023). The miniDOAS data are available here
418 https://iasi-ft.eu/products/nh3_minidoas/ (Viatte, 2023). The ERA-5 data are available via the Climate
419 Data Record (CDR) Copernicus website
420 <https://cds.climate.copernicus.eu/cdsapp#!/search?text=ERA5%20back%20extension&type=dataset>
421 (C3S CDS, 2023). The potential source contribution function is available via the Meteothink.org
422 <http://meteothink.org/docs/trajstat/pscf.html> (Wang et al., 2009). Last access to all URLs: 23 May
423 2023.

424

425 **Author contributions**

426 CV and NG designed the project. MVD and LC provided the IASI data. AH, AW, DS helped with the
427 miniDOAS installation and data acquisition. CV and CD analyzed the data. CV and CD wrote the
428 manuscript draft. All the co-authors reviewed and edited the manuscript. CC wrote proposals to
429 financially support the miniDOAS.

430 **Competing interests**

431 The authors declare that they have no conflict of interest.

432 **Acknowledgments**

433 IASI is a joint mission of EUMETSAT and the Centre National d'Etudes Spatiales (CNES, France). The IASI
434 Level 1C data are distributed in near real time by EUMETSAT through the EUMETCast system
435 distribution. The authors acknowledge the AERIS data infrastructure (<https://www.aeris-data.fr>) for
436 providing access to the IASI Level 1 radiance and Level 2 NH₃ concentration data used in this study.
437 CNES and the AC-SAF (CDOP3) project provided financial support for the miniDOAS acquisition. We
438 thank the NOAA's Air Resources Laboratory (ARL) for providing the HYSPLIT model. Research at ULB
439 was supported by the Belgian State Federal Office for Scientific, Technical and Cultural Affairs (Prodex
440 HIRS) and the Air Liquide Foundation (TAPIR project). LC is Research Associate supported by the Belgian
441 F.R.S.-FNRS. MVD is supported by the FED-tWIN project ARENBERG funded via the Belgian Science
442 Policy Office (BELSPO).

443



444 **References**

- 445 AERIS: NH₃ total column from IASI (Level 2), <https://iasi.aeris-data.fr/NH3/>, last access: 11 May 2023.
- 446 Airparif, 2022 : <https://www.airparif.asso.fr/surveiller-la-pollution/les-emissions>, last access 24 Feb 2023.
- 447
- 448 Akoglu, H.: User's guide to correlation coefficients, *Turkish J. Emerg. Med.*, 18(3), 91–93, doi:<https://doi.org/10.1016/j.tjem.2018.08.001>, 2018.
- 449
- 450 Berkhout, A. J. C., Swart, D. P. J., Volten, H., Gast, L. F. L., Haaima, M., Verboom, H., Stefess, G.,
451 Hafkenscheid, T., and Hoogerbrugge, R.: Replacing the AMOR with the miniDOAS in the ammonia
452 monitoring network in the Netherlands, *Atmos. Meas. Tech.*, 10, 4099–4120,
453 <https://doi.org/10.5194/amt-10-4099-2017>, 2017.
- 454 Biuki, Z. A., Parvin, P. and Aghaei, M.: Satellite remote sensing of particulate matter in the atmosphere
455 of megacities: A case study of Tehran, Iran, *Atmos. Pollut. Res.*, 13(10), 101545,
456 doi:<https://doi.org/10.1016/j.apr.2022.101545>, 2022.
- 457 Cao, H., Henze, D. K., Cady-Pereira, K., McDonald, B. C., Harkins, C., Sun, K., Bowman, K. W., Fu, T.-M.
458 and Nawaz, M. O.: COVID-19 Lockdowns Afford the First Satellite-Based Confirmation That Vehicles
459 Are an Under-recognized Source of Urban NH₃ Pollution in Los Angeles, *Environ. Sci. Technol. Lett.*,
460 doi:10.1021/acs.estlett.1c00730, 2021.
- 461 Cao, H., Henze, D. K., Shephard, M. W., Dammers, E., Cady-Pereira, K., Alvarado, M., Lonsdale, C., Luo,
462 G., Yu, F., Zhu, L., Danielson, C. G. and Edgerton, E. S.: Inverse modeling of NH₃ sources using CrIS
463 remote sensing measurements, *Environ. Res. Lett.*, 15(10), 104082, doi:10.1088/1748-9326/abb5cc,
464 2020.
- 465 Caville et al.: Measurements of ammonia in ambient air and over a controlled artificial source during
466 the AMICA field campaign at a rural site in the Ile-de-France region, *Sensors*, to be submitted, 2023.
- 467 Chatain, M., Chretien, E., Crunaire, S. and Jantzem, E.: Road Traffic and Its Influence on Urban Ammonia
468 Concentrations (France), *Atmosphere (Basel)*, 13(7), doi:10.3390/atmos13071032, 2022.
- 469 CITEPA, 2022: [https://www.citepa.org/wp-content/uploads/publications/cee-](https://www.citepa.org/wp-content/uploads/publications/cee-nu/UNECE_France_mars2022.pdf)
470 [nu/UNECE France mars2022.pdf](https://www.citepa.org/wp-content/uploads/publications/cee-nu/UNECE_France_mars2022.pdf), last access 24 Feb 2023.
- 471 Clarisse, L., Van Damme, M., Hurtmans, D., Franco, B., Clerbaux, C., & Coheur, P.-F.: The diel cycle of
472 NH₃ observed from the FY-4A Geostationary Interferometric Infrared Sounder (GIIRS). *Geophysical*
473 *Research Letters*, 48, e2021GL093010, <https://doi.org/10.1029/2021GL093010>, 2021.
- 474 Clarisse, L., Clerbaux, C., Dentener, F., Hurtmans, D., and Coheur, P.-F.: Global ammonia distribution
475 derived from infrared satellite observations, *Nat. Geosci.*, 2, 479–483,
476 <https://doi.org/10.1038/ngeo551>, 2009.
- 477 Clerbaux, C., Boynard, A., Clarisse, L., George, M., Hadji-Lazaro, J., Herbin, H., Hurtmans, D., Pommier,
478 M., Razavi, A., Turquety, S., Wespes, C. and Coheur, P.-F.: Monitoring of atmospheric composition using
479 the thermal infrared IASI/MetOp sounder, *Atmos. Chem. Phys.*, 9(16), 6041–6054, doi:10.5194/acp-9-
480 6041-2009, 2009.



- 481 Copernicus Climate Change Service, Climate Data Store, (2023): ERA5 hourly data on single levels from
482 1940 to present. Copernicus Climate Change Service (C3S) Climate Data Store (CDS), DOI:
483 10.24381/cds.adbb2d47 (Accessed on 11-May-2023)
- 484 Dammers, E., McLinden, C. A., Griffin, D., Shephard, M. W., Van Der Graaf, S., Lutsch, E., Schaap, M.,
485 Gainairu-Matz, Y., Fioletov, V., Van Damme, M., Whitburn, S., Clarisse, L., Cady-Pereira, K., Clerbaux,
486 C., Coheur, P. F., and Erisman, J. W.: NH₃ emissions from large point sources derived from CrIS and IASI
487 satellite observations, *Atmos. Chem. Phys.*, 19, 12261–12293, [https://doi.org/10.5194/acp-19-12261-](https://doi.org/10.5194/acp-19-12261-2019)
488 2019, 2019.
- 489 Evangeliou, N., Balkanski, Y., Eckhardt, S., Cozic, A., Van Damme, M., Coheur, P.-F., Clarisse, L.,
490 Shephard, M. W., Cady-Pereira, K. E. and Hauglustaine, D.: 10-year satellite-constrained fluxes of
491 ammonia improve performance of chemistry transport models, *Atmos. Chem. Phys.*, 21(6), 4431–
492 4451, doi:10.5194/acp-21-4431-2021, 2021.
- 493 Farren, N. J., Davison, J., Rose, R. A., Wagner, R. L. and Carslaw, D. C.: Underestimated Ammonia
494 Emissions from Road Vehicles, *Environ. Sci. Technol.*, 54(24), 15689–15697,
495 doi:10.1021/acs.est.0c05839, 2020.
- 496 Favez, O., Weber, S., Petit, J.-E., Alleman, L. Y., Albinet, A., Riffault, V., Chazeau, B., Amodeo, T.,
497 Salameh, D., Zhang, Y., Srivastava, D., Samaké, A., Aujay-Plouzeau, R., Papin, A., Bonnaire, N.,
498 Boullanger, C., Chatain, M., Chevrier, F., Detournay, A., Leoz-Garziandia, E. (2021). Overview of the
499 French Operational Network for In Situ Observation of PM Chemical Composition and Sources in Urban
500 Environments (CARA Program), *Atmosphere*, 12(2), <https://doi.org/10.3390/atmos12020207>, 2021.
- 501 Fortems-Cheiney, A., Dufour, G., Dufossé, K., Couvidat, F., Gilliot, J.-M., Siour, G., Beekmann, M., Foret,
502 G., Meleux, F., Clarisse, L., Coheur, P.-F., Van Damme, M., Clerbaux, C., and Génarmont, S.: Do
503 alternative inventories converge on the spatiotemporal representation of spring ammonia emissions
504 in France?, *Atmos. Chem. Phys.*, 20, 13481–13495, <https://doi.org/10.5194/acp-20-13481-2020>, 2020.
- 505 Fowler, D., et al.: The global nitrogen cycle in the twenty-first century, *Philos. Trans. R. Soc. B*,
506 368(1621), 1–13, doi:10.1098/rstb.2013.0164, 2013.
- 507 Ge, X., Schaap, M., Kranenburg, R., Segers, A., Reinds, G. J., Kros, H. and de Vries, W.: Modeling
508 atmospheric ammonia using agricultural emissions with improved spatial variability and temporal
509 dynamics, *Atmos. Chem. Phys.*, 20(24), 16055–16087, doi:10.5194/acp-20-16055-2020, 2020.
- 510 Guo, X., Wang, R., Pan, D., Zondlo, M. A., Clarisse, L., Van Damme, M., Whitburn, S., Coheur, P.-F.,
511 Clerbaux, C., Franco, B., Golston, L. M., Wendt, L., Sun, K., Tao, L., Miller, D., Mikoviny, T., Müller, M.,
512 Wisthaler, A., Tevlin, A. G., Murphy, J. G., Nowak, J. B., Roscioli, J. R., Volkamer, R., Kille, N., Neuman,
513 J. A., Eilerman, S. J., Crawford, J. H., Yacovitch, T. I., Barrick, J. D. and Scarino, A. J.: Validation of IASI
514 Satellite Ammonia Observations at the Pixel Scale Using In Situ Vertical Profiles, *J. Geophys. Res.*
515 *Atmos.*, 126(9), e2020JD033475, doi:<https://doi.org/10.1029/2020JD033475>, 2021.
- 516 Hersbach, H.; Bell, B.; Berrisford, P.; Hirahara, S.; Horányi, A.; Muñoz-Sabater, J.; Nicolas, J.; Peubey,
517 C.; Radu, R.; Schepers, D.; et al. The ERA5 global reanalysis. *Q. J. R. Meteorol. Soc.* 146, 1999–2049,
518 doi:10.1002/qj.3803, <https://www.ecmwf.int/en/forecasts/datasets/reanalysis-datasets/era5>, 2020.



- 519 Hu, Q., Zhang, L., Evans, G. J. and Yao, X.: Variability of atmospheric ammonia related to potential
520 emission sources in downtown Toronto, Canada, *Atmos. Environ.*, 99, 365–373,
521 doi:<https://doi.org/10.1016/j.atmosenv.2014.10.006>, 2014.
- 522 Ianniello, A., Spataro, F., Esposito, G., Allegrini, I., Rantica, E., Ancora, M. P., Hu, M. and Zhu, T.:
523 Occurrence of gas phase ammonia in the area of Beijing (China), *Atmos. Chem. Phys.*, 10(19), 9487–
524 9503, doi:[10.5194/acp-10-9487-2010](https://doi.org/10.5194/acp-10-9487-2010), 2010.
- 525 Jeong, U., Kim, J., Lee, H., Jung, J., Kim, Y. J., Song, C. H. and Koo, J.-H.: Estimation of the contributions
526 of long range transported aerosol in East Asia to carbonaceous aerosol and PM concentrations in
527 Seoul, Korea using highly time resolved measurements: a PSCF model approach, *J. Environ. Monit.*,
528 13(7), 1905–1918, doi:[10.1039/C0EM00659A](https://doi.org/10.1039/C0EM00659A), 2011.
- 529 Kutzner, R. D., Cuesta, J., Chelin, P., Petit, J.-E., Ray, M., Landsheere, X., Tournadre, B., Dupont, J.-C.,
530 Rosso, A., Hase, F., Orphal, J., and Beekmann, M.: Diurnal evolution of total column and surface
531 atmospheric ammonia in the megacity of Paris, France, during an intense springtime pollution episode,
532 *Atmos. Chem. Phys.*, 21, 12091–12111, <https://doi.org/10.5194/acp-21-12091-2021>, 2021.
- 533 Lan, Z., Lin, W., Pu, W. and Ma, Z.: Measurement report: Exploring NH₃ behavior in urban and suburban
534 Beijing: comparison and implications, *Atmos. Chem. Phys.*, 21(6), 4561–4573, doi:[10.5194/acp-21-4561-2021](https://doi.org/10.5194/acp-21-4561-2021), 2021.
- 536 Li, Y., Thompson, T. M., Van Damme, M., Chen, X., Benedict, K. B., Shao, Y., Day, D., Boris, A., Sullivan,
537 A. P., Ham, J., Whitburn, S., Clarisse, L., Coheur, P.-F. and Collett Jr., J. L.: Temporal and spatial variability
538 of ammonia in urban and agricultural regions of northern Colorado, United States, *Atmos. Chem. Phys.*,
539 17(10), 6197–6213, doi:[10.5194/acp-17-6197-2017](https://doi.org/10.5194/acp-17-6197-2017), 2017.
- 540 Lonati, G. and Cernuschi, S.: Temporal and spatial variability of atmospheric ammonia in the Lombardy
541 region (Northern Italy), *Atmos. Pollut. Res.*, 11(12), 2154–2163,
542 doi:<https://doi.org/10.1016/j.apr.2020.06.004>, 2020.
- 543 Lonsdale, C. R., Hegarty, J. D., Cady-Pereira, K. E., Alvarado, M. J., Henze, D. K., Turner, M. D., Capps, S.
544 L., Nowak, J. B., Neuman, J. A., Middlebrook, A. M., Bahreini, R., Murphy, J. G., Markovic, M. Z.,
545 VandenBoer, T. C., Russell, L. M., and Scarino, A. J.: Modeling the diurnal variability of agricultural
546 ammonia in Bakersfield, California, during the CalNex campaign, *Atmos. Chem. Phys.*, 17, 2721–2739,
547 <https://doi.org/10.5194/acp-17-2721-2017>, 2017.
- 548 Loubet, B., Buysse, P., Gonzaga-Gomez, L., Lafouge, F., Ciuraru, R., Decuq, C., Kammer, J., Bsaibes, S.,
549 Boissard, C., Durand, B., Gueudet, J.-C., Fanucci, O., Zurfluh, O., Abis, L., Zannoni, N., Truong, F.,
550 Baisnée, D., Sarda-Estève, R., Staudt, M. and Gros, V.: Volatile organic compound fluxes over a winter
551 wheat field by PTR-Qi-TOF-MS and eddy covariance, *Atmos. Chem. Phys.*, 22(4), 2817–2842,
552 doi:[10.5194/acp-22-2817-2022](https://doi.org/10.5194/acp-22-2817-2022), 2022.
- 553 Ludemann, C. I., Gruere, A., Heffer, P. and Dobermann, A.: Global data on fertilizer use by crop and
554 by country, *Sci. Data*, 9(1), 501, doi:[10.1038/s41597-022-01592-z](https://doi.org/10.1038/s41597-022-01592-z), 2022.
- 555 Malm, W. C., Johnson, C. E., and Bresch, J. F.: Application of principal component analysis for purpose
556 of identifying source receptor relationships, in *Receptor Methods for Source Apportionment*, Pace,
557 T.G., Ed.; Publication TR-5, Air Pollution Control Association, Pittsburgh, PA, pp. 127–148, 1986.
- 558 Marais, E. A., Pandey, A. K., Van Damme, M., Clarisse, L., Coheur, P.-F., Shephard, M. W., Cady-Pereira,
559 K. E., Misselbrook, T., Zhu, L., Luo, G. and Yu, F.: UK Ammonia Emissions Estimated With Satellite



- 560 Observations and GEOS-Chem, *J. Geophys. Res. Atmos.*, 126(18), e2021JD035237,
561 doi:<https://doi.org/10.1029/2021JD035237>, 2021.
- 562 Martino, M., Tassone, A., Angiuli, L., Naccarato, A., Dambruoso, P. R., Mazzone, F., Trizio, L., Leonardi,
563 C., Petracchini, F., Sprovieri, F., Pirrone, N., D'Amore, F. and Bencardino, M.: First atmospheric mercury
564 measurements at a coastal site in the Apulia region: seasonal variability and source analysis, *Environ.*
565 *Sci. Pollut. Res.*, 29(45), 68460–68475, doi:10.1007/s11356-022-20505-6, 2022.
- 566 McDuffie, E. E., Smith, S. J., O'Rourke, P., Tibrewal, K., Venkataraman, C., Marais, E. A., Zheng, B.,
567 Crippa, M., Brauer, M., and Martin, R. V.: A global anthropogenic emission inventory of atmospheric
568 pollutants from sector- and fuel-specific sources (1970–2017): an application of the Community
569 Emissions Data System (CEDS), *Earth Syst. Sci. Data*, 12, 3413–3442, <https://doi.org/10.5194/essd-12-3413-2020>, 2020.
- 571 Nair, A. A. and Yu, F.: Quantification of Atmospheric Ammonia Concentrations: A Review of Its
572 Measurement and Modeling, *Atmosphere (Basel)*, 11(10), doi:10.3390/atmos11101092, 2020.
- 573 Osada, K.: Measurement report: Short-term variation in ammonia concentrations in an urban area
574 increased by mist evaporation and emissions from a forest canopy with bird droppings, *Atmos. Chem.*
575 *Phys.*, 20, 11941–11954, <https://doi.org/10.5194/acp-20-11941-2020>, 2020.
- 576 Pazmiño, A., Beekmann, M., Goutail, F., Ionov, D., Bazureau, A., Nunes-Pinharanda, M., Hauchecorne,
577 A., and Godin-Beekmann, S.: Impact of the COVID-19 pandemic related to lockdown measures on
578 tropospheric NO₂ columns over Île-de-France, *Atmos. Chem. Phys.*, 21, 18303–18317,
579 <https://doi.org/10.5194/acp-21-18303-2021>, 2021.
- 580 Perrino, C., Catrambone, M., Di Menno Di Bucchianico, A. and Allegrini, I.: Gaseous ammonia in the
581 urban area of Rome, Italy and its relationship with traffic emissions, *Atmos. Environ.*, 36(34), 5385–
582 5394, doi:[https://doi.org/10.1016/S1352-2310\(02\)00469-7](https://doi.org/10.1016/S1352-2310(02)00469-7), 2002.
- 583 Petetin, H., et al.: Assessing the ammonium nitrate formation regime in the Paris megacity and its
584 representation in the CHIMERE model, *Atmos. Chem. Phys.*, 16, 10419–10440, doi:10.5194/acp-16-
585 10419-2016, 2016.
- 586 Pu, W., Sheng, J., Tian, P., Huang, M., Liu, X., Collett, J. L., Li, Z., Zhao, X., He, D., Dong, F., Zhang, N.,
587 Quan, W., Qiu, Y., Song, Y., Lin, W., Pan, Y. and Ma, Z.: On-road mobile mapping of spatial variations
588 and source contributions of ammonia in Beijing, China, *Sci. Total Environ.*, 864, 160869,
589 doi:<https://doi.org/10.1016/j.scitotenv.2022.160869>, 2023.
- 590 Pope III, C. A., et al.: Fine-particulate air pollution and life expectancy in the United States, *N. Engl. J.*
591 *Med.*, 360(4), 376–386, doi:10.1056/NEJMsa0805646, 2009.
- 592 Qadri, A. M., Singh, G. K., Paul, D., Gupta, T., Rabha, S., Islam, N. and Saikia, B. K.: Variabilities of $\delta^{13}C$
593 and carbonaceous components in ambient PM_{2.5} in Northeast India: Insights into sources and
594 atmospheric processes, *Environ. Res.*, 214, 113801,
595 doi:<https://doi.org/10.1016/j.envres.2022.113801>, 2022.
- 596 Ren, B., Xie, P., Xu, J., Li, A., Tian, X., Hu, Z., Huang, Y., Li, X., Zhang, Q., Ren, H. and Ji, H.: Use of the
597 PSCF method to analyze the variations of potential sources and transports of NO₂, SO₂, and HCHO
598 observed by MAX-DOAS in Nanjing, China during 2019, *Sci. Total Environ.*, 782, 146865,
599 doi:<https://doi.org/10.1016/j.scitotenv.2021.146865>, 2021.



- 600 Rockström, J., Steffen, W., Noone, K., Persson, Å., Chapin, F. S., Lambin, E. F., Lenton, T. M., Scheffer,
601 M., Folke, C., Schellnhuber, H. J., Nykvist, B., de Wit, C. A., Hughes, T., van der Leeuw, S., Rodhe, H.,
602 Sörlin, S., Snyder, P. K., Costanza, R., Svedin, U., Falkenmark, M., Karlberg, L., Corell, R. W., Fabry, V. J.,
603 Hansen, J., Walker, B., Liverman, D., Richardson, K., Crutzen, P. and Foley, J. A.: A safe operating space
604 for humanity, *Nature*, 461(7263), 472–475, doi:10.1038/461472a, 2009.
- 605 Roe, S.; Spivey, M.; Lindquist, H.; Thesing, K.; Strait, R.; Pechan, E.; Associates, I. Estimating Ammonia
606 Emissions from Anthropogenic Nonagricultural Sources. EPA Emission Inventory Improvement
607 Program. Technical Report; Emission Inventory Improvement Program, 2004.
- 608 Shephard, M.W., and Cady-Pereira, K.E.: Cross-track Infrared Sounder (CrIS) satellite observations of
609 tropospheric ammonia, *Atmos. Meas. Tech.*, 8, 1323-1336, 2015.
- 610 Stein, A. F., Draxler, R. R., Rolph, G. D., Stunder, B. J. B., Cohen, M. D. and Ngan, F.: NOAA's HYSPLIT
611 Atmospheric Transport and Dispersion Modeling System, *Bull. Am. Meteorol. Soc.*, 96(12), 2059–2077,
612 doi:10.1175/BAMS-D-14-00110.1, 2015.
- 613 Sudesh, S, and Kulshrestha, U. C. Diurnal Variation of Ambient NH₃ in Relation with Agricultural
614 Activities and Meteorological Factors at a Rural Site in North India. *Curr World Environ*, SI1.
615 DOI:<http://dx.doi.org/10.12944/CWE.16.Special-Issue1.02>, 2021.
- 616 Sun, K., Tao, L., Miller, D. J., Pan, D., Golston, L. M., Zondlo, M. A., Griffin, R. J., Wallace, H. W., Leong,
617 Y. J., Yang, M. M., Zhang, Y., Mauzerall, D. L. and Zhu, T.: Vehicle Emissions as an Important Urban
618 Ammonia Source in the United States and China, *Environ. Sci. Technol.*, 51(4), 2472–2481,
619 doi:10.1021/acs.est.6b02805, 2017.
- 620 Sutton, M. A., Reis, S., Riddick, S. N., Dragosits, U., Nemitz, E., Theobald, M. R., Tang, Y. S., Braban, C.
621 F., Vieno, M., Dore, A. J., Mitchell, R. F., Wanless, S., Daunt, F., Fowler, D., Blackall, T. D., Milford, C.,
622 Flechard, C. R., Loubet, B., Massad, R., Cellier, P., Personne, E., Coheur, P. F., Clarisse, L., Van Damme,
623 M., Ngadi, Y., Clerbaux, C., Skjøth, C. A., Geels, C., Hertel, O., Wichink Kruit, R. J., Pinder, R. W., Bash, J.
624 O., Walker, J. T., Simpson, D., Horváth, L., Misselbrook, T. H., Bleeker, A., Dentener, F. and de Vries, W.:
625 Towards a climate-dependent paradigm of ammonia emission and deposition, *Philos. Trans. R. Soc.*
626 *Lond. B. Biol. Sci.*, 368(1621), 20130166, doi:10.1098/rstb.2013.0166, 2013.
- 627 Sutton, M.; Dragosits, U.; Tang, Y.; Fowler, D.: Ammonia emissions from nonagricultural sources in the
628 UK. *Atmos. Environ.* 34, 855– 869, DOI: 10.1016/S1352-2310(99)00362-3, 2000.
- 629 Twigg, M. M., Berkhout, A. J. C., Cowan, N., Crunaire, S., Dammers, E., Ebert, V., Gaudion, V., Haaima,
630 M., Häni, C., John, L., Jones, M. R., Kamps, B., Kentisbeer, J., Kupper, T., Leeson, S. R., Leuenberger, D.,
631 Lüttschwager, N. O. B., Makkonen, U., Martin, N. A., Missler, D., Mounsor, D., Neftel, A., Nelson, C.,
632 Nemitz, E., Oudwater, R., Pascale, C., Petit, J.-E., Pogany, A., Redon, N., Sintermann, J., Stephens, A.,
633 Sutton, M. A., Tang, Y. S., Zijlmans, R., Braban, C. F., and Niederhauser, B.: Intercomparison of in situ
634 measurements of ambient NH₃: instrument performance and application under field conditions,
635 *Atmos. Meas. Tech.*, 15, 6755–6787, <https://doi.org/10.5194/amt-15-6755-2022>, 2022.
- 636 Van Damme, M., Clarisse, L., Stavrou, T., Wichink Kruit, R., Sellekaerts, L., Viatte, C., Clerbaux, C. and
637 Coheur, P.-F.: On the weekly cycle of atmospheric ammonia over European agricultural hotspots, *Sci.*
638 *Rep.*, 12(1), 12327, doi:10.1038/s41598-022-15836-w, 2022.



- 639 Van Damme, M., Clarisse, L., Franco, B., Sutton, M. A., Erisman, J. W., Wichink Kruit, R., van Zanten,
640 M., Whitburn, S., Hadji-Lazaro, J., Hurtmans, D., Clerbaux, C., & Coheur, P.-F.: Global, regional and
641 national trends of atmospheric ammonia derived from a decadal (2008–2018) satellite record.
642 *Environmental Research Letters*, 16(5), 55017. <https://doi.org/10.1088/1748-9326/abd5e0>, 2021.
- 643 Van Damme, M., Clarisse, L., Whitburn, S., Hadji-Lazaro, J., Hurtmans, D., Clerbaux, C. and Coheur, P.-
644 F.: Industrial and agricultural ammonia point sources exposed, *Nature*, 564(7734), 99–103,
645 doi:10.1038/s41586-018-0747-1, 2018.
- 646 Van Damme, M., Clarisse, L., Dammers, E., Liu, X., Nowak, J. B., Clerbaux, C., Flechard, C. R., Galy-
647 Lacaux, C., Xu, W., Neuman, J. A., Tang, Y. S., Sutton, M. A., Erisman, J. W. and Coheur, P. F.: Towards
648 validation of ammonia (NH₃) measurements from the IASI satellite, *Atmos. Meas. Tech.*, 8(3), 1575–
649 1591, doi:10.5194/amt-8-1575-2015, 2015.
- 650 Viatte, C. (2023). NH₃ from Mini Doas [Data set]. LATMOS.
- 651 Viatte, C., Abeer, R., Yamanouchi, S., Porter, W. C., Safieddine, S., Van Damme, M., Clarisse, L., Herrera,
652 B., Grutter, M., Coheur, P.-F., Strong, K. and Clerbaux, C.: NH₃ spatiotemporal variability over Paris,
653 Mexico City, and Toronto, and its link to PM_{2.5} during pollution events, *Atmos. Chem. Phys.*, 22(19),
654 12907–12922, doi:10.5194/acp-22-12907-2022, 2022.
- 655 Viatte, C., Petit, J.-E., Yamanouchi, S., Van Damme, M., Doucerain, C., Germain-Piaulenne, E., Gros, V.,
656 Favez, O., Clarisse, L., Coheur, P.-F., Strong, K. and Clerbaux, C.: Ammonia and PM_{2.5} air pollution in
657 paris during the 2020 covid lockdown, *Atmosphere*, 12(2), doi:10.3390/atmos12020160, 2021.
- 658 Viatte, C., Wang, T., Van Damme, M., Dammers, E., Meleux, F., Clarisse, L., Shephard, M. W., Whitburn,
659 S., François Coheur, P., Cady-Pereira, K. E. and Clerbaux, C.: Atmospheric ammonia variability and link
660 with particulate matter formation: A case study over the Paris area, *Atmos. Chem. Phys.*, 20(1),
661 doi:10.5194/acp-20-577-2020, 2020.
- 662 Volten, H., Bergwerff, J. B., Haaime, M., Lolkema, D. E., Berkhout, A. J. C., van der Hoff, G. R., Potma,
663 C. J. M., Wichink Kruit, R. J., van Pul, W. A. J. and Swart, D. P. J.: Two instruments based on differential
664 optical absorption spectroscopy (DOAS) to measure accurate ammonia concentrations in the
665 atmosphere, *Atmos. Meas. Tech.*, 5(2), 413–427, doi:10.5194/amt-5-413-2012, 2012.
- 666 von Bobruzki, K., Braban, C. F., Famulari, D., Jones, S. K., Blackall, T., Smith, T. E. L., Blom, M., Coe, H.,
667 Gallagher, M., Ghalaieny, M., McGillen, M. R., Percival, C. J., Whitehead, J. D., Ellis, R., Murphy, J.,
668 Mohacsi, A., Pogany, A., Junninen, H., Rantanen, S., Sutton, M. A. and Nemitz, E.: Field inter-
669 comparison of eleven atmospheric ammonia measurement techniques, *Atmos. Meas. Tech.*, 3(1), 91–
670 112, doi:10.5194/amt-3-91-2010, 2010.
- 671 Wang, B., Liu, Z., Li, Z., Sun, Y., Wang, C., Zhu, C., Sun, L., Yang, N., Bai, G., Fan, G., Sun, X., Xia, Z., Pan,
672 G., Xu, C. and Yan, G.: Characteristics, chemical transformation and source apportionment of volatile
673 organic compounds (VOCs) during wintertime at a suburban site in a provincial capital city, east China,
674 *Atmos. Environ.*, 298, 119621, doi:<https://doi.org/10.1016/j.atmosenv.2023.119621>, 2023.



- 675 Wang, S., Nan, J., Shi, C., Fu, Q., Gao, S., Wang, D., Cui, H., Saiz-Lopez, A. and Zhou, B.: Atmospheric
676 ammonia and its impacts on regional air quality over the megacity of Shanghai, China, *Sci. Rep.*, 5(1),
677 15842, doi:10.1038/srep15842, 2015.
- 678 Wang, Y.Q., Zhang, X.Y. and Draxler, R.:TrajStat: GIS-based software that uses various trajectory
679 statistical analysis methods to identify potential sources from long-term air pollution measurement
680 data. *Environmental Modelling & Software*, 24: 938-939, 2009.
- 681 Warner, J. X., Wei, Z., Strow, L. L., Dickerson, R. R., and Nowak, J. B.: The global tropospheric ammonia
682 distribution as seen in the 13-year AIRS measurement record, *Atmos. Chem. Phys.*, 16, 5467-5479,
683 <https://doi.org/10.5194/acp-16-5467-2016>, 2016.
- 684 Wen, Y., Zhang, S., Wu, Y. and Hao, J.: Vehicular ammonia emissions: An underappreciated emission
685 source in densely-populated areas, *Atmos. Chem. Phys. Discuss.*, 2022, 1–14, doi:10.5194/acp-2022-
686 828, 2022.
- 687 Whitehead, J., Longley, D., Coe, H. and Gallagher, M.: Hourly concentrations of ammonia during the
688 winter in Manchester, UK, related to traffic and background sources, Fifth Conference on Urban
689 Environment, Session 14 urban air quality (including urban airshed modeling and urban air chemistry
690 experiments), Vancouver BC, Canada, 23-26 August 2004.
- 691 Zachary, M., Yin, L. and Zacharia, M.: Application of PSCF and CWT to Identify Potential Sources of
692 Aerosol Optical Depth in ICIPE Mbita. *Open Access Library Journal*, 5, 1-12. doi: 10.4236/oalib.1104487,
693 2018.
- 694 Zhang, Q., Wei, N., Zou, C. and Mao, H.: Evaluating the ammonia emission from in-use vehicles using
695 on-road remote sensing test, *Environ. Pollut.*, 271, 116384,
696 doi:<https://doi.org/10.1016/j.envpol.2020.116384>, 2021.